

Thermodynamic Investigation of Metamagnetism in Pulsed High Magnetic Fields on Heavy Fermion Superconductor UTe_2

Shusaku Imajo^{1*}, Yoshimitsu Kohama¹, Atsushi Miyake¹, Chao Dong¹, Masashi Tokunaga¹, Jacques Flouquet², Koichi Kindo¹, and Dai Aoki^{2,3}

¹The Institute for Solid State Physics, University of Tokyo, Kashiwa, Chiba 277-8581, Japan

²University Grenoble Alpes, CEA, IRIG-PHELIQS, F-3800 Grenoble, France

³Institute for Materials Research, Tohoku University, Oarai, Ibaraki 311-1313, Japan

We investigated the thermodynamic property of the heavy fermion superconductor UTe_2 in pulsed high magnetic fields. The superconducting transition in zero field was observed at $T_c=1.65$ K as a sharp heat capacity jump. Magnetocaloric effect measurements in pulsed-magnetic fields obviously detected a thermodynamic anomaly accompanied by a first-order metamagnetic transition at $\mu_0 H_m=36.0$ T when the fields are applied nearly along the hard-magnetization b -axis. From the results of heat capacity measurements in magnetic fields, we found a drastic diverging electronic heat capacity coefficient of the normal state γ_N with approaching H_m . Comparing with the previous works via the magnetic Clausius-Clapeyron relation, we unveil the thermodynamic details of the metamagnetic transition. The enhancement of the effective mass observed as the development of γ_N indicates that quantum fluctuation strongly evolves around H_m ; it assists the superconductivity emerging even in extremely high fields.

The occurrence of unconventional triplet superconductivity (SC) in ferromagnetic (FM) compounds begins with the discovery of superconductivity in UGe_2 ¹⁾ with the singularity that SC emerges just at the crossing between two FM phases (FM2 and FM1) at a pressure $P_x \sim 1.2$ GPa; it collapses on entering in the paramagnetic (PM) ground state above $P_c \sim 1.6$ GPa. Lowering the Curie temperature in UGe_2 ($T_{Curie} = 52$ K) and $URhGe$ ($T_{Curie} = 9.5$ K) leads to the opportunity to modify the ferromagnetic interactions by the magnetic field.^{2,3)} A spectacular phenomenon observed in $URhGe$ ⁴⁾ is that transverse magnetic field ($H \parallel b$, hard magnetization axis) with respect to the ferromagnetic sublattice magnetization ($M \sim 0.4 \mu_B$, $H \parallel c$ -axis, easy-magnetization axis) pushes T_{Curie} to zero at a spin-reorientation field $\mu_0 H_R \sim 12$ T and the field-reentrant superconductivity (RSC) appears between 8 to 13 T.^{5,6)} The origin of RSC is the field enhancement of the effective mass m^* ,^{7,8)} which may result from the combined effects of ferromagnetic fluctuations and Fermi surface instabilities associated with the Lifshitz transition.⁹⁾ Metamagnetic transition in itinerant ferromagnetic materials is often connected with the so called wing structure of PM-FM boundary close to the critical pressure P_c in the phase diagram. In uranium compounds, well-known cases are UGe_2 ^{10,11)} and $UCoAl$,^{12,13)} when the field is applied along the Ising easy-magnetization axis. As it is known in $URhGe$, a new key phenomenon in UTe_2 is the field evolution of the magneto-crystalline energy.

The new feature with the discovery of SC in UTe_2 is that the ground state in the normal state is paramagnetic at the verge of FM order.¹⁴⁻¹⁶⁾ When the field is applied along the b -axis in the orthorhombic structure, a sharp metamagnetic transition occurs at $\mu_0 H_m = 35$ T,¹⁷⁻¹⁹⁾ leading to a polarized ferromagnetic phase with a huge jump $\Delta M \sim 0.6 \mu_B$ of the magnetization,¹⁷⁾ which is six times larger than that of $URhGe$ ($\Delta M \sim 0.1 \mu_B$).⁵⁾ In UTe_2 , at low field, the easy-magnetization axis is now a -axis; above H_m the b -axis be-

comes the easy-magnetization axis. The strong enhancement of SC is observed as the field increases towards H_m .^{19,20)} Our aim is to present direct heat capacity measurements down to 0.8 K at lower temperature, comparing with the previous estimation of the field variation of m^* . We focus on the field dependence of the linear temperature term of the heat capacity (γ_N), which is proportional to the effective mass m^* , that is, $m^* = m^{**} + m_b$, where m_b is the band mass and m^{**} is the correlation mass driven by ferromagnetic fluctuations but also by additional Fermi surface instabilities at H_m . The coupling constant of the Cooper pair is given by $\lambda = m^{**}/m_b$.²⁾

A single crystal of UTe_2 was grown using chemical vapor transport method.^{14,15)} Measurements of heat capacity on the single crystal of UTe_2 , weighing 444.6 μg , were performed by the quasi-adiabatic method²⁻⁴⁾ in highly stabilized magnetic fields¹⁾ generated by a long pulse magnet at the International MegaGauss Science Laboratory of the Institute for Solid State Physics of the University of Tokyo. The details of the heat capacity measurements are described in the supplemental materials.²⁵⁾ The b -axis of the sample was parallel to the direction of the applied field within an accuracy of a few degrees. Measurements of magnetocaloric effect on the same single crystal were also performed by using the same calorimeter. This measurement can be regarded as both nearly isothermal and adiabatic conditions depending on the time scale of magnetocaloric effect. For a sudden magnetocaloric effect enough less than the external relaxation time τ_1 , the field dependence of temperature $T(H)$ mimics an adiabatic (isentropic) process.

As a first characterization of the low-temperature electronic state, we report the temperature dependence of the heat capacity at 0 T in Fig. 1. The superconducting transition is clearly observed at $T_c \sim 1.65$ K as a sharp jump of heat capacity. Above T_c , the temperature dependence is well described by the conventional Fermi liquid behavior of the heat capacity, $C_p/T = \gamma_N + \beta T^2$. The Sommerfeld coefficient γ_N and lattice heat capacity coefficient β are estimated as 123.5 ± 0.3 mJK⁻²mol⁻¹ and 2.81 ± 0.02 mJK⁻⁴mol⁻¹, respectively. The

*imajo@issp.u-tokyo.ac.jp

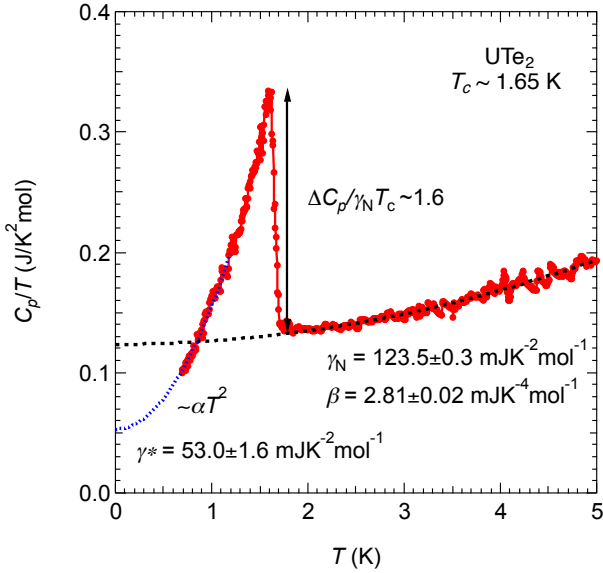


Fig. 1. (Color online) Temperature dependence of low-temperature heat capacity of a single crystal of UTe_2 at 0 T plotted as C_p/T vs. T . The black dotted curve indicates a least square fit to the equation, $C_p/T = \gamma_N + \beta T^2$, with the electronic heat capacity coefficient of the normal state γ_N and the lattice heat capacity coefficient β . The blue dotted curve represents a low-temperature extrapolation by $C_p/T = \gamma^* + \alpha T^2$, where γ^* denotes the residual electronic heat capacity coefficient of the superconducting state and the T^2 term corresponds typical quasi-particle excitation expected for point-node superconductors.

value of γ_N agrees well with the reported values.^{14,15)} The sharp thermodynamic anomaly accompanied by the superconducting transition is also reproduced consistently with the previous works,^{14,15)} which confirms the bulk superconductivity and the high quality of the present sample. The height of the heat capacity jump at T_c , $\Delta C_p / \gamma_N T_c$ may appear to reach about 1.6, which is slightly larger than the value, 1.43, expected for the BCS-type weak-coupling superconductivity. At lower temperatures, the early reports succeed to represent the temperature dependence by using $C_p/T = \gamma^* + \alpha T^2$, which is known as the temperature dependence of C_p in the point-nodal superconductors with the residual electronic heat capacity coefficient γ^* . A least square fit to our data over the temperature range 0.7 K to 1.2 K yields $\gamma^* = 53.0 \pm 1.6 \text{ mJ K}^{-2} \text{ mol}^{-1}$, in good agreements with the previous reports.^{14,15)} If the half of the density of states in the normal state is related with the formation of the superconductivity, the height of the heat capacity jump at T_c gives $\Delta C_p / (\gamma_N - \gamma^*) T_c = 2.8$; a solid evidence for the strong-coupling superconductivity in UTe_2 .

Next we turn our attention to the focus of this work, namely, understanding of the thermodynamic property of the metamagnetic transition. Figure 2 shows the magnetocaloric effect observed in smoothly changing magnetic fields. A sudden temperature step in the ascending part of the field pulse ΔT_{up} is observed at ~ 36.1 T, attributable to the metamagnetic transition, while the step is again detected at ~ 36.0 T in the descending process as ΔT_{down} . The sign of the temperature steps for both ascending and descending magnetic fields is positive, implying that the metamagnetic transition is considered as a first-order phase transition which release a large hysteresis loss as well as a latent heat.²⁶⁾ The difference between the

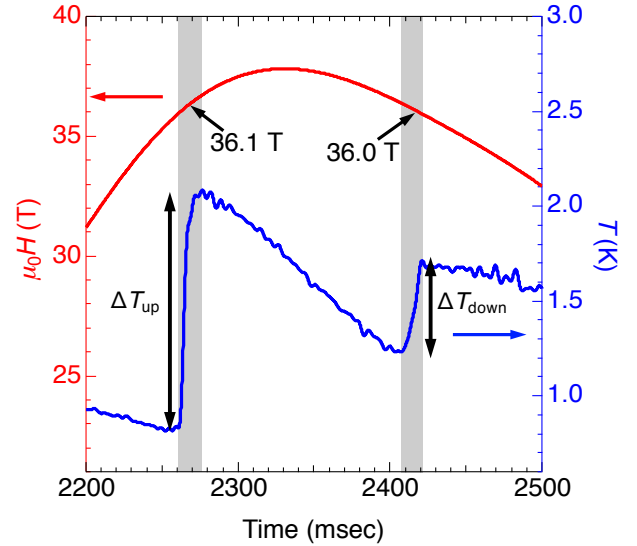


Fig. 2. (Color online) Time profiles of magnetic field and temperature in a magnetocaloric effect measurement in a pulsed-field. At the shaded areas, the sudden heating ΔT_{up} and ΔT_{down} are observed when the magnetic field reaches about 36.0–36.1 T. The time scale of the heating is ~ 10 ms that is much less than τ_1 , implying that the temperature change at the phase boundary can be treated as a nearly adiabatic process.

temperature steps, ΔT_{up} and ΔT_{down} , could be explained by the latent heat concomitant with the first-order phase transition because the sign of the entropy change and thus the sign of heat release are opposite depending on whether the field is in the descending or ascending field pulse. From the MCE experiment, we also notice that the present value of the critical field of 36.0–36.1 T is slightly higher than the reported values of $\mu_0 H_m$ (~ 34.9 T,¹⁷⁾ ~ 35.5 T,¹⁸⁾ ~ 35 T¹⁹⁾). The deviation of the transition field can be caused by the small misalignment of the applied magnetic fields from the crystallographic b -axis. The angle dependence of H_m has been recently reported.¹⁹⁾

In order to further explore the metamagnetic transition, we carried out the heat capacity measurements in pulsed magnetic fields up to 38.1 T, which are shown in Fig. 3. At 11.5 T, the higher temperature tail associated with the superconducting transition still remains below 1 K. The persistence of the superconductivity against magnetic fields agrees with the exceptionally high upper critical fields,^{14,15,19,20)} in which the RSC up to H_m were reported for the perfect field-alignment along b -axis. In the normal state, the intercepts of C_p/T at $T = 0$ K progressively increase as field increase and show a peak at H_m , followed by the decrease at higher fields. Since the intercept of C_p/T directly corresponds to γ_N , this indicates that γ_N shows a peak at H_m . We should point out that the present C_p data above H_m are missing below 1.5 K due to the large heating effect at H_m as shown in Fig. 2. One can still extrapolate the data and confirms that the γ_N decreases on the either side of H_m . In order to follow the field dependence of γ_N in more detail, we present the normalized electronic contribution $\gamma_N(\mu_0 H) / \gamma_N(0 \text{ T})$ as a function of the normalized magnetic field H/H_m in Fig. 4. For comparison with earlier works, the normalized electronic contribution estimated by the magnetization measurement,¹⁷⁾ and the square root of the normalized quadratic term A of the electrical resistivity¹⁸⁾ are also shown in Fig. 4. Here, the

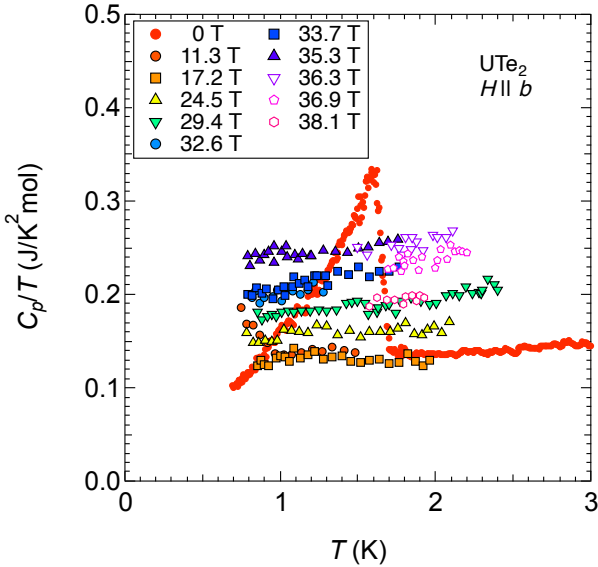


Fig. 3. (Color online) Temperature dependence of heat capacity plotted as the C_p/T vs. T at various magnetic fields. The thermodynamic anomaly below 1 K at 11.5 T originates from the superconducting transition. The extrapolations of the data points to zero temperature yields γ_N for each fields. No contribution from the nuclear heat capacity was observed for the present study.

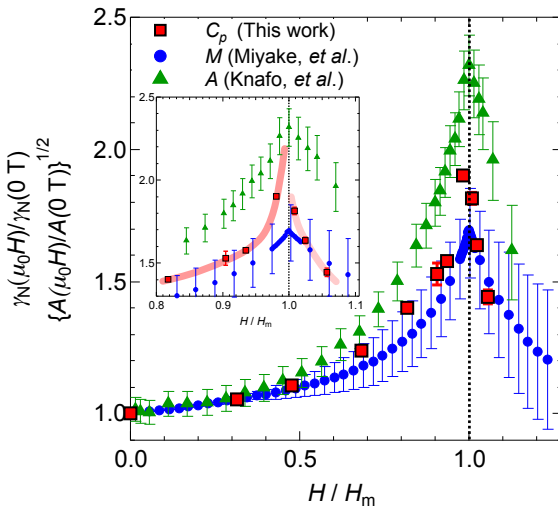


Fig. 4. (Color online) Magnetic field dependence of γ_N with scaling by γ_N at 0 T and the metamagnetic transition field H_m . The red boxes and blue circles represent $\gamma_N(\mu_0 H)/\gamma_N(0 T)$ measured in this work and estimated in the magnetization study,¹⁷⁾ respectively. The green triangles denote the square root of the normalized quadratic term A obtained in the electrical resistivity measurement.¹⁸⁾ The inset shows the enlarged plot around H_m and the thick red curves are guides for the eyes.

square root of A is assumed to be proportional to the electronic heat capacity coefficient γ_N for a Fermi-liquid system, following the Kadowaki-Woods relation, which is often obeyed in heavy fermion compounds.²⁷⁾ However, through ferromagnetic-paramagnetic instability crossing the Stoner factor $I = 1$, A is predicted to diverge in $1/(1 - I)$ while γ varies as $\ln(1 - I)$.²⁸⁾ Thus, the differences between \sqrt{A} and γ are expected. The γ_N rapidly increase with approaching H_m ,

and the extrapolated value of γ_N to H_m is found to be more than twice ($\gamma_N(\mu_0 H_m) \sim 250 \text{ mJK}^{-2} \text{ mol}^{-1}$) at H_m than that at zero magnetic field. The diverging behavior toward H_m qualitatively agrees with the earlier reports.^{17,18)} We notice however there are a few quantitative differences; the asymmetry of γ_N around H_m and the absolute value of $\gamma_N(\mu_0 H_m)/\gamma_N(0 T)$. The most plausible explanation for these discrepancies is the range of the measurement temperature. This work estimates the density of state with the low temperature heat capacity from 0.8 to 2.5 K, while the resistivity (1.5 to 4.2 K) and magnetization (4.2 to 9.0 K) uses the data obtained relatively higher temperature region. The earlier magnetization and resistivity measurements assume an isothermal condition for estimating the electronic density of state from field scan data. The assumption might be broken with a rapid field sweep rate of pulsed fields, especially for UTe_2 due to the large temperature rise at H_m (See Fig. 2).

For the characterization of the metamagnetic transition, we roughly evaluate the latent heat and the hysteresis loss from the present results. At the phase transition illustrated as the shaded area in Fig. 2, we simply assume that the sample is in an adiabatic condition because the time-scale of the phase transition is about 10 msec that is much shorter than the external relaxation time (>100 msec). In such cases, the entropy change ΔS can be expressed as the following formula,^{26,29)}

$$\Delta S = -C_p \Delta T/T + \delta Q_{\text{loss}}/T, \quad (1)$$

where δQ_{loss} represents the hysteresis loss. This gives the estimates of the latent heat ΔS_m and hysteresis loss δQ_{loss} as the half of the difference between the up-sweep and down-sweep results and the average of the up-sweep and down-sweep results, respectively. Here, we assume the constant value of $C_p/T = 250 \text{ mJK}^{-2} \text{ mol}^{-1}$ because C_p/T is almost independent on temperature below 2 K even though the value should have some temperature, field dependences and be influenced by the difference between the up-sweep and down-sweep due to the hysteresis. Since the ambiguity of the value is estimated as $\sim 10\%$ by the discontinuity at H_m in the inset of Fig. 4, our estimations should be accurate within the error margin of 10%. While the latent heat of the metamagnetic transition ΔS_m is given as $\sim -90 \text{ mJK}^{-1} \text{ mol}^{-1}$, the δQ_{loss} reaches $\sim 320 \text{ mJmol}^{-1}$ when T is about 1.5 K. Using the relation of the hysteresis loss, $\delta Q_{\text{loss}} = \Delta M \Delta H$, where $\Delta H = 0.1 \text{ T}$ is the width of the hysteresis, the size of ΔM is given as $\Delta M = 0.6 \mu_B/\text{f.u.}$, which is well consistent with the reported magnetization jump.^{17,19)} Moreover, the ΔS_m is also found to be fairly consistent with the value $-70 \text{ mJK}^{-1} \text{ mol}^{-1}$ calculated by using the magnetic Clausius-Clapeyron equation, $\Delta S_m = -\Delta M(d(\mu_0 H_m)/dT)$, with the slope of the reported phase boundary, $d(\mu_0 H_m)/dT$ of 20 mT/K ^{17,18)} (the phase boundary is determined by the midpoints of the transition lines in the up-sweep and down-sweep processes), and the magnetization jump, ΔM of $0.6 \mu_B/\text{f.u.}$ Although these analyses depend on the sample quality and measurement condition, the fulfillment of the relation confirms the reliability of our analysis and implies that the change in the entropy is predominately the magnetic origin. If we take the latent heat as $\sim -90 \text{ mJK}^{-1} \text{ mol}^{-1}$, γ_N should show discontinuity with a step at H_m , where the γ_N of the higher-field state ($>H_m$) becomes smaller than that in the lower-field state ($<H_m$). As seen in the inset of Fig. 4, our data are not sufficient to clearly see

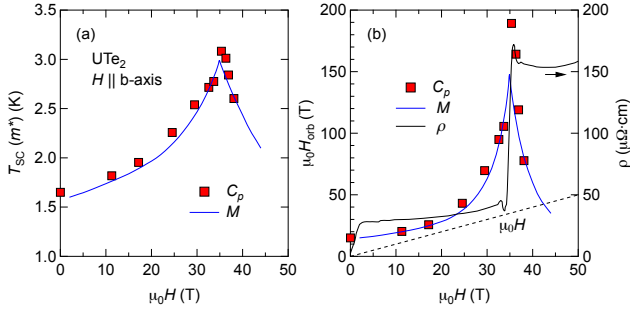


Fig. 5. (Color online) (a) Calculated T_{SC} as a function of field obtained from the heat capacity and magnetization¹⁷⁾ measurements in UTe_2 . (b) Calculated orbital limits (left-axis) and electrical resistivity¹⁸⁾ (right-axis) as a function of field. The orbital limits are obtained by the formula $H_{orb} \sim (m^*T_{SC})^2$ from the data of the heat capacity and magnetization¹⁷⁾ measurements.

the discontinuity, but the γ_N of the higher-field state tends to be smaller than that of the lower-field state. This finding that the electronic entropy below the critical field is higher than that above the critical field has an implication for the nature of the high field electronic state. Figure 5(a) shows the field dependence of T_{SC} derived from heat capacity and magnetization data by using a simplified McMillan-type formula,^{2,7,8,17)} $T_{SC} = T_0 \exp\left(-\frac{\lambda+1}{\lambda}\right)$, where T_0 is a constant determined by the experimental T_{SC} at 0 T, with a parameter chosen in Ref. 17, assuming m_b is field-independent. Figure 5(b) emphasizes the huge enhancement of the orbital limit H_{orb} by a factor ~ 13 close to H_m , assuming H_{orb} proportional to $(m^*T_{SC})^2$. Let us remark that H_{c2} becomes closer to the applied field H in the field range between 12 and 25 T, where RSC is observed for the perfect H alignment along b -axis. For $H \parallel b$, superconductivity disappears above H_m . Two main mechanisms are: i) change of Fermi surface with an enhancement of m_b and thus a drop of λ above H_m , ii) drastic decrease of the mean free path l above H_m , leading to the collapse of superconductivity. A remarkable phenomenon is the jump of the magnetoresistance at 1.5 K just on entering into the polarized ferromagnetic phase.²⁰⁾ If we assume that ρ just above H_m is related to the electronic disorder going from PM to FM ground state, $T_{SC}(m_H^*)/T_{SC}(m_{H=0}^*)$ is boosted by a factor 2, while ρ is jumped by a factor 5. It is worthwhile to remember the difficulty to evaluate A in a clean material when the crossover from collision regime to collisionless regime at $\omega_c\tau$ reaches 1, where $\omega_c (= e(\mu_0H)/(m^*c))$ is cyclotron frequency, $\tau (\propto l)$ is the scattering life time. Fortunately just around H_m , $\omega_c\tau$ drops by a factor near 10 due to the increase of m^* and the decrease of l . In order to clarify the angular dependence of superconducting stability in the PM and polarized FM phases, important ingredients are the angular dependence of $m^*(\mu_0H)$, $m_b(\mu_0H)$ and $l(\mu_0H)$. Note that it is established that field misalignment to a -axis leads to a fast increase of H_m associated to a collapse of RSC, as it occurs in URhGe,⁵⁾ while misalignment to c -axis leads to a weak increase of H_m and stabilization of a superconducting ferromagnetic domain as observed in UGe_2 .³⁰⁾ From previous studies on heavy fermion compounds³¹⁾ and extensive measurements on the link between $m^*(\mu_0H_m)$ and $\rho(\mu_0H_m)$ in URhGe,^{5-8,32,33)} the reappearance of SC in FM phase may be explained.

In summary, we studied the thermodynamic properties of the heavy fermion superconductor UTe_2 in pulsed high magnetic fields applied parallel to the b -axis so as to elucidate the details of the recently reported metamagnetic transition.¹⁷⁻¹⁹⁾ As reported in the previous works,^{14,15)} we confirm the large electronic heat capacity coefficient of the normal state, $\gamma_N = 123.5 \pm 0.3 \text{ mJK}^{-2} \text{ mol}^{-1}$, at 0 T. The sharp heat capacity jump by the superconducting transition at $T_c \sim 1.65$ K is also reproduced. From the results of the magnetocaloric effect in pulsed-fields, we detect the thermodynamic anomaly at ~ 36.0 T. The heat capacity measurements in pulsed high fields reveal the diverging behavior of γ_N toward H_m , although the superconducting transition cannot be detected above 11.5 T due to the slight tilt of the b -axis from the field direction. Using the present results, the details of the metamagnetic transition is clarified as a first-order transition with the latent heat and hysteresis loss and we quantitatively succeed to demonstrate the magnetization work^{17,19)} through the magnetic Clausius-Clapeyron relation. The significant development of γ_N directly indicates the enhancement of m^* linked to FM instability driven at H_m . Qualitatively the RSC can be well explained by the field dependence of m^* and the feedback on the electronic mean free path. As the future issues, the pairing mechanism of the superconductivity including symmetry of the gap function should be investigated. A clear continuation of our thermodynamic studies is to detect the $m^*(\mu_0H)$ singularities in the SC-FM domain detected with a misalignment along c -axis.

Acknowledgment This work was supported by KAKENHI (JP15H05884, JP15H05882, JP15K21732, JP16H04006, JP15H05745).

- 1) S.S. Saxena, P. Agarwal, K. Ahilan, F.M. Grosche, R.K.W. Haselwimmer, M.J. Steiner, E. Pugh, I.R. Walker, S.R. Julian, P. Monthoux, G.G. Lonzarich, A. Huxley, I. Sheikin, D. Braithwaite and J. Flouquet, *Nature* **406**, 587 (2000).
- 2) D. Aoki, K. Ishida and J. Flouquet, *J. Phys. Soc. Jpn.* **88**, 022001 (2019).
- 3) D. Aoki and J. Flouquet, *J. Phys. Soc. Jpn.* **81**, 011003 (2012).
- 4) D. Aoki, A. Huxley, E. Ressouche, D. Braithwaite, J. Flouquet, J.-P. Brison, E. Lhotel and C. Paulsen, *Nature* **413**, 613 (2001).
- 5) F. Lévy, I. Sheikin, B. Grenier and A.D. Huxley, *Science* **309**, 1343 (2005).
- 6) F. Lévy, I. Sheikin and A. Huxley, *Nature Physics* **3**, 460 (2007).
- 7) A. Miyake, D. Aoki and J. Flouquet, *J. Phys. Soc. Jpn.* **77**, 094709 (2008).
- 8) A. Miyake, D. Aoki and J. Flouquet, *J. Phys. Soc. Jpn.* **78**, 063703 (2009).
- 9) Y. Sherkunov, A.V. Chubukov and J.J. Betouras, *Phys. Rev. Lett.* **121**, 097001 (2018).
- 10) V. Taufour, D. Aoki, G. Knebel and J. Flouquet, *Phys. Rev. Lett.* **105**, 217201 (2010).
- 11) H. Kotegawa, V. Taufour, D. Aoki, G. Knebel and J. Flouquet, *J. Phys. Soc. Jpn.* **80**, 083703 (2011).
- 12) D. Aoki, T. Combier, V. Taufour, T.D. Matsuda, G. Knebel, H. Kotegawa and J. Flouquet, *J. Phys. Soc. Jpn.* **80**, 094711 (2011).
- 13) N. Kimura, N. Kabeya, H. Aoki, K. Ohyama, M. Maeda, H. Fujii, M. Kogure, T. Asai, T. Komatsubara, T. Yamamura and I. Satoh, *Phys. Rev. B* **92**, 035106 (2015).
- 14) S. Ran, C. Eckberg, Q.-P. Ding, Y. Furukawa, T. Metz, S. R. Saha, I. -L. Liu, M. Zic, H. Kim, J. Paglione, and N. P. Butch, arXiv:1811.11808.
- 15) D. Aoki, A. Nakamura, F. Honda, D. X. Li, Y. Homma, Y. Shimizu, Y. J. Sato, G. Knebel, J.-P. Brison, A. Pourret, D. Braithwaite, G. Lapertot, Q. Niu, M. Vališka, H. Harima, and J. Flouquet, *J. Phys. Soc. Jpn.* **88**, 043702 (2019).
- 16) S. Sundar, S. Gheidi, K. Akintola, A. M. Côté, S. R. Dunsiger, S. Ran,

- N. P. Butch, S. R. Saha, J. Paglione, and J. E. Sonier, arXiv:1905.06901.
- 17) A. Miyake, Y. Shimizu, Y. J. Sato, D.X. Li, A. Nakamura, Y. Homma, F. Honda, J. Flouquet, M. Tokunaga, and D. Aoki, *J. Phys. Soc. Jpn.* **88**, 063706 (2019).
 - 18) W. Knafo, M. Vališka, D. Braithwaite, G. Lapertot, G. Knebel, A. Pourret, J.-P. Brison, J. Flouquet, D. Aoki, *J. Phys. Soc. Jpn.* **88**, 063705 (2019).
 - 19) S. Ran, I.-L. Liu, Y. S. Eo, D. J. Campbell, P. Neves, W. T. Fuhrman, S. R. Saha, C. Eckberg, H. Kim, J. Paglione, D. Graf, J. Singleton and N. P. Butch, arXiv:1905.04343.
 - 20) G. Knebel, W. Knafo, A. Pourret, Q. Niu, M. ValiÅka, D. Braithwaite, G. Lapertot, M. Nardone, A. Zitouni, S. Mishra, I. Sheikin, G. Seyfarth, J.-P. Brison, D. Aoki, and J. Flouquet, *J. Phys. Soc. Jpn.* **88**, 063707 (2019).
 - 21) Y. Kohama, Y. Hashimoto, S. Katsumoto, M. Tokunaga and K. Kindo, *Meas. Sci. Technol.* **24**, 115005 (2013).
 - 22) Y. Kohama, H. Ishikawa, A. Matsuo, K. Kindo, N. Shannon, and Z. Hiroi, *Proc. Natl. Acad. Sci. USA*, **116** 10686 (2019).
 - 23) L. Jiao, M. Smidman, Y. Kohama, Z. S. Wang, D. Graf, Z. F. Weng, Y. J. Zhang, A. Matsuo, E. D. Bauer, Hanoh Lee, S. Kirchner, J. Singleton, K. Kindo, J. Wosnitza, F. Steglich, J. D. Thompson, and H. Q. Yuan, *Phys. Rev. B* **99**, 045127 (2019).
 - 24) Y. Kohama, and K. Kindo, *Rev. Sci. Instrum.* **86**, 104701 (2015).
 - 25) (Supplemental Material) The details of the present heat capacity measurements are provided online.
 - 26) A. V. Silhanek, M. Jaime, N. Harrison, V. R. Fanelli, C. D. Batista, H. Amitsuka, S. Nakatsuji, L. Balicas, K. H. Kim, Z. Fisk, J. L. Sarrao, L. Civale, and J. A. Mydosh, *Phys. Rev. Lett.* **96**, 136403 (2006).
 - 27) K. Kadowaki and S. B. Woods, *Solid State Commun.* **58**, 507 (1986).
 - 28) T. Moriya, *Acta Phys. Pol. B* **34**, 287 (2003).
 - 29) Y. Aoki, T. D. Matsuda, H. Sugawara, H. Sato, H. Ohkuni, R. Settai, Y. Ōnuki, E. Yamamoto, Y. Haga, A. V. Andreev, V. Sechovsky, L. Havela, H. Ikeda, K. Miyake, *J. Magn. Magn. Mater.* **177-181**, 271 (1998).
 - 30) I. Sheikin, A. Huxley, D. Braithwaite, J.P. Brison, S. Watanabe, K. Miyake and J. Flouquet, *Phys. Rev. B* **64**, 220503 (2001).
 - 31) J. Flouquet, P. Haen, F. Lapierre, C. Fierz, A. Amato and D. Jaccard, *J. Magn. Magn. Mater.* **76&77**, 285 (1988).
 - 32) F. Hardy, D. Aoki, C. Meingast, P. Schweiss, P. Burger, H. v. Loehneysen and J. Flouquet, *Phys. Rev. B* **83**, 195107 (2011).
 - 33) S. Nakamura, T. Sakakibara, Y. Shimizu, S. Kittaka, Y. Kono, Y. Haga, J. Pospíšil and E. Yamamoto, *Phys. Rev. B* **96**, 094411 (2017).

Supplemental Material for Thermodynamic Investigation of Metamagnetism in Pulsed High Magnetic Fields on Heavy Fermion Superconductor UTe_2

In this supplemental material, the details of heat capacity measurements under pulsed magnetic fields are presented. Measurements of heat capacity in pulsed magnetic fields were performed in highly stabilized magnetic fields generated by the specially designed long pulsed magnet. The pulsed magnet was composed of a main coil and an additional mini-coil to generate highly stabilized magnetic fields for several hundreds milliseconds with a feedback control technique.¹⁾ Fig. S6(a),(d) show a typical magnetic field profile used for this research, where the total time duration of pulse is ~ 1.3 sec. The field stability during heat capacity measurements on the top of field pulse is within ~ 0.002 T. To obtain the absolute value of heat capacity, we employed the quasi-adiabatic method.²⁻⁴⁾ The calorimeter consists of liquid ^3He thermal bath, $\text{Pt}_{0.92}\text{W}_{0.08}$ thermal relaxation wires and TiO_2 substrate to which RuO_2 resistors for a heater and a thermometer are attached. The single crystal of UTe_2 was mounted on the substrate of the calorimeter with Apiezon N grease.

As seen in Fig. S6(d-f), the heat capacity measurements were carried out within the stabilized field region, where each data point was obtained in 10 msec with a 1 msec heat pulse. The duration of measurement time scale of 10 ms was enough shorter than the external relaxation time τ_1 that was the order of 100 msec. The internal relaxation time of the sample τ_2 was about one millisecond as seen in the rapid thermal relaxation after the application of the heat pulse (see Fig. S6(e)). We can avoid the effect of τ_2 by using the data after the completion of the internal relaxation as illustrated by the red dotted lines. Therefore, the present condition, $\tau_2 \ll 10 \text{ msec} \ll \tau_1$, is suitable for the quasi-adiabatic method and the heat capacity is simply given as $C_p = \Delta Q / \Delta T$ where ΔQ and ΔT are total

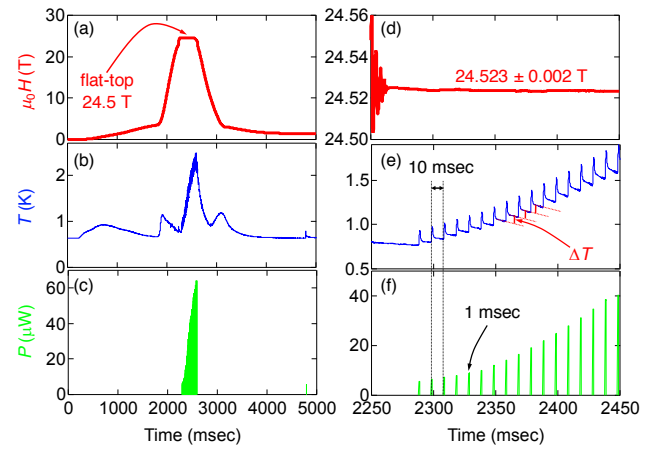


Fig. S6. (Color online) Quasi-adiabatic heat capacity experiment in the long pulsed magnet. (a) Time dependence of magnetic field profile, (b) Sample temperature, (c) applied power as a function of time. (d),(e),(f) are the enlarged plots of (a),(b),(c), respectively, for the stabilized field region from 2250 to 2450 ms. In each 10 msec temperature step, heat capacity is measured by the simple equation $C_p = \Delta Q / \Delta T$, where ΔQ is a total of the applied heat quantity in each heat pulse.

amount of applied heat and temperature increment, respectively.

- 1) Y. Kohama, and K. Kindo, Rev. Sci. Instrum. **86**, 104701 (2015).
- 2) Y. Kohama, Y. Hashimoto, S. Katsumoto, M. Tokunaga and K. Kindo, Meas. Sci. Technol. **24**, 115005 (2013).
- 3) Y. Kohama, H. Ishikawa, A. Matsuo, K. Kindo, N. Shannon, and Z. Hiroi, Proc. Natl. Acad. Sci. USA, **116**, 10686 (2019).
- 4) L. Jiao, M. Smidman, Y. Kohama, Z. S. Wang, D. Graf, Z. F. Weng, Y. J. Zhang, A. Matsuo, E. D. Bauer, Hanoh Lee, S. Kirchner, J. Singleton, K. Kindo, J. Wosnitzer, F. Steglich, J. D. Thompson, and H. Q. Yuan, Phys. Rev. B **99**, 045127 (2019).